IEEE Access
Multidisciplinary | Rapid Review | Open Access Journal

Received May 21, 2021, accepted June 11, 2021, date of publication June 21, 2021, date of current version June 28, 2021.

Digital Object Identifier 10.1109/ACCESS.2021.3090804

Divergence Measure on a Modified Sprott-C System

ENZENG DONG[1], HUI YU[1], JIGANG TONG[1], AND ZENGHUI WANG[2], (Member, IEEE)

[1]Tianjin Key Laboratory For Control Theory and Applications in Complicated Systems, Tianjin University of Technology, Tianjin 300384, China
[2]Department of Electrical and Mining Engineering, University of South Africa, Florida 1710, South Africa

Corresponding author: Jigang Tong (tjgtjut@163.com)

This work was supported in part by the Natural Science Foundation of Tianjin under Grant 18JCYBJC87700, in part by the New Generation Artificial Intelligence Technology Major Project of Tianjin under Grant 18ZXZNSY00270, in part by the South African National Research Foundation under Grant 132797, and in part by the South African National Research Foundation Incentive under Grant 114911.

ABSTRACT In this paper, a modified Sprott-C chaotic system is proposed based on Kolmogrov model, which shows rich dynamic behaviors, especially, the system divergence is related to the variables. To quantitatively evaluate the influence of variable divergence on phase space volume, the ultimate bound and equilibrium point of the system are analyzed and two indicators are proposed. The study shows that the volume of the phase space of the system contracts when the initial divergence is less than 0, while the volume expands first and then contracts when the initial divergence is greater than 0. The influence of the variable divergence on the system is revealed. Furthermore, it is shown that the stability of equilibrium point has no effect on the divergence on the phase space volume.

INDEX TERMS Divergence, equilibrium point, ultimate boundary.

I. INTRODUCTION

Chaos refers to the uncertain or unpredictable randomness of a certain nonlinear system under certain conditions, and is known as one of the ''three revolutions'' in the natural science of the 20th century [1]. Since Lorenz discovered the first chaotic attractor in the 1960s [2], Chaos as an important branch of nonlinear system theory, has been developing rapidly and gradually become a hot research topic in the field of modern natural science. In addition, chaos has obtained huge and far-reaching achievements in different research areas, such as stability and bifurcation analysis [3]–[7], coexistence attractor and hidden attractor [8]–[13], chaos control and chaos synchronization [14]–[17], dynamic behavior analysis of memristors, neural network [18]–[22], and so on. After understanding the general laws of chaos, the research of chaos began to develop into the application field [23]–[28].

The ultimate bound plays an important role in the qualitative behavior research of a chaotic system [29]–[31], and it has a wide range of applications in the control and synchronization of chaos. Since the Lorenz system was proposed, many researchers have been working on the ultimate bound of Lorenz system. It was not until 1987 that Leonov, a Russian scholar, gave a ultimate bound in the form of ellipsoid and cylinder for the first time [32]. Subsequently, many scholars studied the ultimate bounds of different chaotic systems and obtained the ultimate bounds of some chaotic systems, such as Lorenz system [33]–[37], Lorenz system family [38]–[40], Chen system [41], Chua system [42], Lorenz-Haken system [43], and so on.

From the point of view of the volume of phase space, the chaotic systems can be divided into volume conservative chaos and volume variable chaos [44]. The divergence can be used to describe the divergence degree of vector field of each point in space [45]–[47]. When the divergence $divF > 0$, the volume expansion of phase space indicates that the attractor is generated by a positive source. When $divF < 0$, the volume contraction of phase space indicates that the attractor is generated by a negative source. When $divF = 0$, the volume of the phase space is constant, the system is a volume conservative chaos and there is no attractor. The divergence of most chaotic systems is a fixed value, but some system divergences are affected by the system variables. However, there are few studies on the influence of system variables on chaotic system divergence. To evaluate the divergence of a system, it would be important to have some indicators, and this paper proposes two indicators to measure the system divergence.

The associate editor coordinating the review of this manuscript and approving it for publication was Di He.

In this paper, a modified dissipative system is proposed based on the Sprott-C system [48]. The Kolmogorov form is used to analyze the mechanism of the system [49]–[54], and then the stability and ultimate bounds of the system are analyzed [55], [56]. It is found that the divergence of the system is not a fixed value but related to variables, which is analyzed in this paper since the divergence is rarely analyzed. The main contributions of this paper are: 1) the classical Sprott-C system is modified to a dissipative system whose divergence is affected by variables; 2) we analyze the equilibrium point and the ultimate bound of the system, and the analysis results are used to analyze the divergence affected by variables; 3) two new indicators are proposed to analyze the dissipative system affected by variables.

The rest of this paper is organized as follows. In Sect. 2, a modified Sprott-C dissipative system is proposed and some basic dynamics have been analyzed. In Sect. 3, the mechanism of the system is analyzed. In Sect. 4, some basic characteristics of equilibrium points are analyzed and the ultimate boundary of the system is estimated. In Sect. 5, the system's divergence is analyzed, when initial points is outside the ultimate bound, based on two proposed divergence indicators. Finally, conclusion is drawn in Sect. 6.

II. A MODIFIED CHAOTIC SYSTEM

In 1994, Sprott [48] proposed a series of simple three-dimensional autonomous systems through a large number of numerical experiments. These systems are similar to Lorenz model, but have different attractor shapes and chaotic characteristics, and the Sprott-C system is

$$\begin{cases} \dot{x} = yz \\ \dot{y} = x - y \\ \dot{z} = 1 - x^2 \end{cases} \tag{1}$$

The system (1) can be represented as

$$\begin{bmatrix} \dot{x} \\ \dot{y} \\ \dot{z} \end{bmatrix} = \begin{bmatrix} 0 & z & 0 \\ 0 & 0 & 0 \\ -x & 0 & 0 \end{bmatrix} \times \begin{bmatrix} x \\ y \\ z \end{bmatrix} + \begin{bmatrix} 0 & 0 & 0 \\ 0 & -1 & 0 \\ 0 & 0 & 0 \end{bmatrix} \times \begin{bmatrix} x \\ y \\ z \end{bmatrix} + \begin{bmatrix} 0 \\ x \\ 1 \end{bmatrix}, \tag{2}$$

and its Kolmogrov form is

$$\dot{X} = J(x)\nabla H + \Lambda X + f, \tag{3}$$

where $J(x)$ is the structure matrix, Λ is the dissipative torque and f is the outer ideal. In this paper, a new system is proposed by modifying $J(x)$ and Λ. The structure matrix $J(x)$ of the system (1) can be modified as

$$J(x) = \begin{bmatrix} 0 & z & bx \\ -z & 0 & -ex \\ -x & ex & 0 \end{bmatrix} \tag{4}$$

Obviously, when $abcde \neq 0, b = 1$ and $d = 1 + e$, the structure matrix $J(x)$ is skew-symmetric. Here, Λ can be

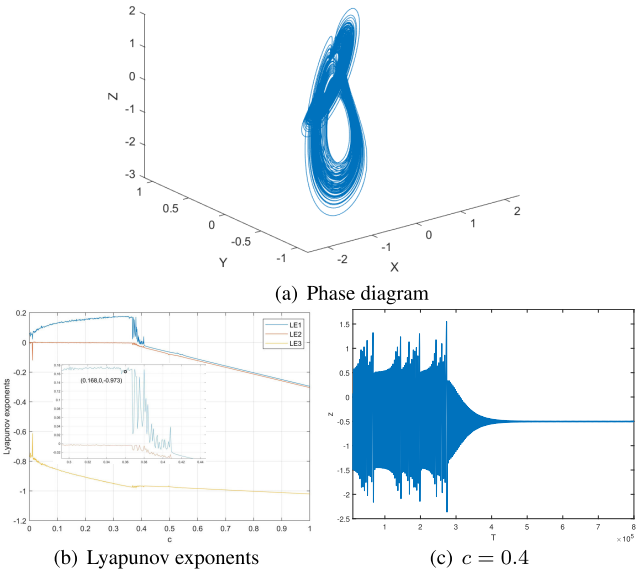

(a) Phase diagram

(b) Lyapunov exponents (c) $c = 0.4$

FIGURE 1. Nonlinear system with chaotic dynamics.

modified as

$$\Lambda = \begin{bmatrix} -a & 0 & 0 \\ 0 & -1 & 0 \\ 0 & 0 & -c \end{bmatrix}$$

Then, the new system can be expressed as

$$\begin{cases} \dot{x} = yz - ax + bxz \\ \dot{y} = x - y - dxz \\ \dot{z} = 1 - x^2 - cz + exy \end{cases} \tag{5}$$

When $abcde \neq 0, a = -0.88, b = 1, c = 0.36, d = -0.5$ and $e = -1.5$, the phase diagram and Lyapunov exponents (LEs) of the system (5) are shown in Fig. 1, and it can be seen from Fig. 1(b) that the LEs are $(0.168, 0, -0.973)$, which show the system (5) is chaotic with the given parameters. And with the increase of parameter c, the maximum LE of the system gradually increases, and when the parameter $c > 0.367$, the maximum LE of the system oscillates and gradually decreases to below 0, which means the system converges to the equilibrium point through transient chaos with the increase of the parameter c, as shown in Fig. 1(c).

Considering the symmetric transformation, it can be found that the system (5) is invariant under $T : (x, y, z) \rightarrow (-x, -y, z)$, and the solutions of the system (5) is z-symmetric in the state space. The projection of the symmetrical image on the coordinate plane can be expressed as central symmetry or axial symmetry. More precisely, it is centrosymmetric in the $x - y$ plane, and z-axis symmetry in the $y - z$ and $x - z$ planes.

And it can find that the divergence of system (1) is a fixed constant as

$$\nabla \cdot V = \frac{\partial \dot{x}}{\partial x} + \frac{\partial \dot{y}}{\partial y} + \frac{\partial \dot{z}}{\partial z} = -1 \tag{6}$$

However, the divergence of the proposed system is related to the variable z, which means the system divergence is not a

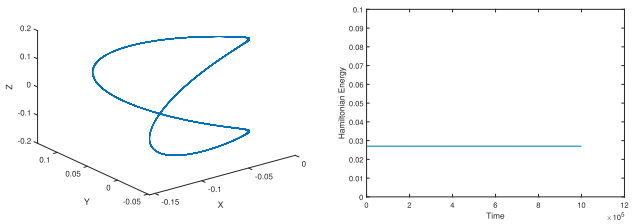

(a) Phase diagram (b) Hamiltonian energy

FIGURE 2. System (5) under inertial torque when $b = 1$, $d = -0.5$ and $e = -1.5$.

fixed constant. Here, the divergence of the system (5) can be expressed as

$$\nabla \cdot V = \frac{\partial \dot{x}}{\partial x} + \frac{\partial \dot{y}}{\partial y} + \frac{\partial \dot{z}}{\partial z} = -a + z - 1 - c \tag{7}$$

III. ENERGY ANALYSIS

The vector field of the system could be decomposed into kinetic torque, internal torque, dissipative torque and external torque. Correspondingly, kinetic energy, potential energy, dissipative energy, and external energy are identified in the system. The kinetic torque can be expressed as

$$K = \frac{1}{2}\left(X^2 + Y^2 + Z^2\right) \tag{8}$$

Let the internal torque be $U = 0$, the dissipative torque and external torque are

$$\Lambda = \begin{bmatrix} \Lambda_1 = -a & 0 & 0 \\ 0 & \Lambda_2 = -1 & 0 \\ 0 & 0 & \Lambda_3 = -c \end{bmatrix} \text{and} f = \begin{bmatrix} 0 \\ x \\ 1 \end{bmatrix}$$

The mechanics of the system (5) is investigated by contrasting it with the Kolmogorov system. When $U = 0$, the system can be expressed as

$$\dot{X} = J(x)\nabla H + \Lambda X + f \tag{9}$$

With the system (5) being represented in terms of its three forms of torques, the system (5) is analyzed under the action of the kinetic, dissipative and external torques, respectively.

A. SYSTEM UNDER INERTIAL TORQUE

When the system (5) is only under the action of inertial torque, the system becomes

$$\dot{X} = J(x)\nabla H \tag{10}$$

When $b = 1, d = -0.5$ and $e = -1.5$, the phase diagram and Hamiltonian energy of the system (5) are shown in Fig. 2.

It can be seen from Fig. 2 that the phase space volume and Hamiltonian energy of the system are conservative.

B. SYSTEM UNDER INERTIAL TORQUE AND EXTERNAL TORQUES

When the system (5) is under the inertial torque and external torques. The phase diagram and Hamiltonian energy of the system (5) are shown in Fig. 3.

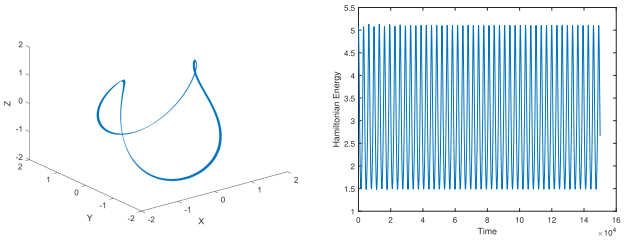

(a) The phase diagram (b) The Hamiltonian energy

FIGURE 3. System under inertial torque and external torque.

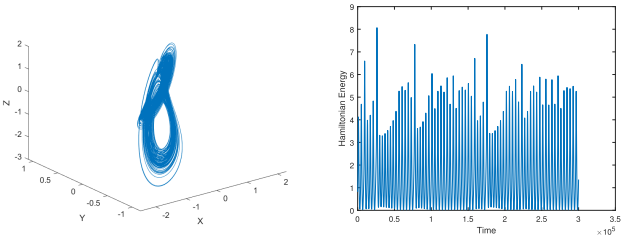

(a) The phase diagram (b) The Hamiltonian energy

FIGURE 4. System under all torques.

It can be seen from Fig. 3 that under the action of inertial torque and external torque, the Hamiltonian energy of the system is periodic and no longer a constant.

C. SYSTEM UNDER ALL TORQUES

When the system (5) is under all torque. The phase diagram and Hamiltonian energy of the system (5) are shown in Fig. 4.It can be seen from Fig. 4 that the system is chaotic under the action of all torques, and the Hamiltonian energy of the system is chaotic.

Through energy analysis, it can be seen that under the action of different torques, the system is in different states. When the system under inertial torque, the system volume and Hamiltonian energy are both conservative; when the system under inertial torque and external torque, the system Hamiltonian energy is periodic; when the system under all torques, the system volume conservation is broken and the Hamiltonian energy becomes more disordered, and the system is chaotic.

IV. EQUILIBRIUM POINT AND BOUNDARY ESTIMATION

In order to further analyze the influence of the divergence on the system dynamics, the ultimate bound and equilibrium point of the system are analyzed first, when the initial point is outside the ulitmate bound, and exclude the influence of the stability of the equilibrium point.

A. EQUILIBRIUM POINT

To analyze the local dynamic characteristics of the system with the change of parameter c, without loss of generality, the following parameters settings: $abcde \neq 0, a = -0.88$, $b = 1, d = -0.5$ and $e = -1.5$ are used, and changing the parameter c. By calculation, the distribution of the system equilibrium points are given in Table 1.

TABLE 1. Distribution of system equilibrium points.

Value range of c	Number	Equilibrium points
$c < -1.987$	3	E_0, E_1, E_2
$-1.99 \leq c \leq -0.286$	5	E_0, E_1, E_2, E_3, E_4
$c > -0.286, c \neq 0$	3	E_0, E_3, E_4

TABLE 2. Basic characteristics of E_0.

Value range of c	Type of Equilibrium point	Stability
$c \leq -1.695$	Saddle point	Unstable
$-1.695 < c < -0.501$	Saddle-focus	Unstable
$-0.501 \leq c < 0$	Saddle point	Unstable
$c > 0$	Saddle point	Unstable

Here,

$$E_0 = \left(0,\ 0,\ \frac{1}{c}\right) \tag{11}$$

$$E_{1,2} = \left\{\mp\sqrt{(28.24c + 8.16)},\ \pm\sqrt{15c + 4.57},\ -3.48\right\} \tag{12}$$

and

$$E_{3,4} = \left\{\pm\sqrt{0.237c + 0.47},\ \mp\sqrt{0.133c + 0.264}\ ,\ -0.5\right\} \tag{13}$$

First, considering E_0, the characteristics of equilibrium point E_0 can be shown in Table 2.

Next, the characteristics of the equilibrium points $E_{1,2}$ are discussed. As $E_{1,2}$ are symmetric about the z-axis, we only focus on E_1.

In this case, the characteristic equation of Jacobian matrix of E_1 is

$$\begin{aligned} &f(\lambda) \\ &= \lambda^3 + (c + 3.617)\lambda^2 \\ &\quad - (3.5\sqrt{(28.54c + 8.16)(16c + 4.57)} + 29.3 + 98.86c)\lambda \\ &\quad - 1.497 - 5.233c + 0.245\sqrt{(28.54c + 8.16)(16c + 4.57)} \end{aligned} \tag{14}$$

It can be observed that the characteristic equation can be expressed as

$$f(\lambda) = a_1\lambda^3 + b_1\lambda^2 + d_1\lambda + e_1 \tag{15}$$

So the eigenvalues of E_1 is calculated by Cardano formula as

$$\begin{aligned} a_1 &= 1, \\ b_1 &= c + 3.617, \\ d_1 &= -98.86c + 3.5\sqrt{(28.54c + 8.2)(16c - 4.57)} - 29.3, \\ e_1 &= 0.245\sqrt{(-28.54c - 8.2)(16c - 4.57)} - 5.23c - 1.5, \\ w &= \frac{-1 + \sqrt[3]{3}i}{2}, \\ p &= \frac{3a_1d_1 - b_1^2}{3a_1^2}, \\ q &= \frac{27a_1^2e_1 - 9a_1b_1d_1 + 2b_1^3}{27a_1^3}, \\ \beta_1 &= \sqrt[3]{\sqrt{\left(\frac{q}{2}\right)^2 + \left(\frac{p}{3}\right)^3} - \frac{q}{2}}, \\ \beta_2 &= \sqrt[3]{\frac{q}{2} + \sqrt{\left(\frac{q}{2}\right)^2 + \left(\frac{p}{3}\right)^3}}, \\ \lambda_1 &= \beta_1 - \beta_2 - \frac{b_1}{3a_1}, \\ \lambda_2 &= w\beta_1 - w^2\beta_2 - \frac{b_1}{3a_1}, \end{aligned}$$

and,

$$\lambda_3 = w^2\beta_1 - w\beta_2 - \frac{b_1}{3a_1},$$

Here, $\lambda_1+\lambda_2+\lambda_3 = -b_1$, which can be proved by follows.

$$\begin{aligned} f(\lambda) &= (\lambda - \lambda_1)(\lambda - \lambda_2)(\lambda - \lambda_3) \\ &= \lambda^3 - (\lambda_1 + \lambda_2 + \lambda_3)\lambda^2 - \lambda_1\lambda_2\lambda_3 \\ &\quad + (\lambda_1\lambda_2 + \lambda_1\lambda_3 + \lambda_2\lambda_3)\lambda \end{aligned} \tag{16}$$

Comparing (15) with (16), the equation $\lambda_1+\lambda_2+\lambda_3 = -b_1$ can be obtained.

If there are $\lambda_3 = -(c + 3.617)$ and $\lambda_{1,2} = \pm\omega i$ at critical stability, taking λ_3 into $f(\lambda)$ obtains

$$\begin{aligned} f(\lambda_3) &= \left(3.5\sqrt{(28.54c+8.2)(16c+4.6)} + 29.3\right)(c + 3.6) \\ &\quad - 5.23c + 0.245\sqrt{(28.54c + 8.2)(16c + 4.6)} \\ &\quad + 98.9c(c + 3.62) - 1.5 = 0 \end{aligned} \tag{17}$$

By solving the equation (17), we can get $c_{h1} = -0.3357$ and $c_{h2} = -3.175$. Here, these two values are to be discussed.

1) When $c = c_{h1}$, obviously, $Re(\lambda_3) \neq 0$,

$$\left.\frac{dRe(\lambda_{1,2})}{dc}\right|_{c=c_{h1}} = 6.395 \neq 0$$

can be obtained by the complex symbolic calculation. So Hopf bifurcation occurs in the system when $c = c_{h1}$. With the growth of parameter c, the stability of the equilibrium point E_1 changes from instability to stability.

2) When $c = c_{h2}$, obviously, $Re(\lambda_3) \neq 0$,

$$\left.\frac{dRe(\lambda_{1,2})}{dc}\right|_{c=c_{h1}} = 1.278 \neq 0$$

can be obtained by the complex symbolic calculation, which means Hopf bifurcation occurs in the system, and the stability of the equilibrium point E_1 changes from stability to instability.

Through the above discussion, the basic characteristics of E_1 can be concluded in Table 3

Then, the basic characteristics of equilibrium point E_3 are analyzed, and the characteristic equation of Jacobian

TABLE 3. Basic characteristics of E_1.

Value range of c	Type of Equilibrium point	Stability
$c < -3.18$	Saddle point	Unstable
$c = -3.18$	Hopf bifurcation point	Hopf bifurcation occurs
$-3.18 < c < -0.336$	Saddle-focus	stable
$c = -0.336$	Hopf bifurcation point	Hopf bifurcation occurs

TABLE 4. Basic characteristics of E_3.

Value range of c	Type of Equilibrium point	Stability
$-1.987 < c \leq -1.632$	Saddle point	Unstable
$-1.632 < c < 0.34$	Saddle-focus	Unstable
$c = 0.34$	Hopf bifurcation point	Hopf bifurcation occurs
$c > 0.34$	Saddle-focus	stable

TABLE 5. Basic characteristics of equilibrium points.

Value range of c	Number	Stability	Unstability
$-8 \leq c < -3.18$	3	0	E_0,$E_{1,2}$
$-3.18 < c < -1.987$	3	$E_{1,2}$	E_0
$-1.987 < c < -0.336$	5	$E_{1,2}$	E_0,$E_{3,4}$
$-0.336 < c < -0.286$	5	0	E_0,$E_{1,2}$,$E_{3,4}$
$-0.286 < c < 0.34$	3	0	E_0,$E_{3,4}$
$0.34 < c < -2.86$	3	$E_{3,4}$	E_0

matrix at E_3 is

$$f(\lambda) = \lambda^3 + (c + 0.62)\lambda^2 + (2.1 + 2.93)\lambda + 1.51c + 3 \tag{18}$$

Using Cardano formula, we can also get the eigenvalues of E_3 and the value of c when Hopf bifurcation occurs. By calculation, $c_{h3} = 0.3403$ and $c_{h4} = -1.640$ can be obtained. Next, the dynamic characteristics of the system for different c values will be discussed.

When $c = c_{h3}$, obviously, $Re(\lambda_3) \neq 0$ and one obtains

$$\left.\frac{dRe(\lambda_{1,2})}{dc}\right|_{c=c_{h3}} = -2.152 \neq 0$$

by the complex symbolic calculation, which means Hopf bifurcation occurs in the system, and the stability of the equilibrium point E_3 changes from instability to stability.

However, when $c = c_{h4}$, $Re(\lambda_3) \neq 0$, $\lambda_{1,2} = \pm\omega i$ are not conjugate pure imaginary, so Hopf bifurcation does not occur in the system. Through the above analysis, the characteristics of E_3 can be shown in Table 4.

Through the above analysis, the basic characteristics of the equilibrium point can be summarized in Table. 5.

B. BOUNDARY ESTIMATION

The ultimate boundary of chaotic system not only plays a key role in the control of chaotic systems, but also can be used to estimate the Hausdorff dimension, so the estimation of the ultimate boundary has great significance. The ultimate bound of the system (5) is to be estimated.

Theorem 1: When $abcde \neq 0$, the trajectory of the system (5) is contained in the ellipsoid

$$\Omega = \left\{(x, y, z) \,|x^2 + y^2 + (z - 1/e)^2 \leq R^2\right\} \tag{19}$$

where

$$R = \max\left\{\left(\frac{1-c/e}{c}\right)^2, \left(\frac{1-bc}{c}\right)^2, \frac{(1-c/e)^2}{4(c-1)}, \frac{(1-c/e)^2}{4(c-a+1/e)^2(a-1/e)}\right\} \tag{20}$$

Proof: Firstly, we construct

$$F(x, y, z) = A_1(x - B_1)^2 + A_2(y - B_2)^2 + A_3(z - B_3)^2 \tag{21}$$

The derivative of $F(x, y, z)$ is

$$\frac{\dot{F}}{2} = A_1(x - B_1)\dot{x} + A_2(y - B_2)\dot{y} + A_3(z - B_3)\dot{z} \tag{22}$$

And the ultimate boundarys must be symmetric about the z-axis as the proposed system is symmetric about the z-axis, the calculation can be simplified by setting

$$A_1 = A_2 = A_3 = 1, \quad B_1 = B_2 = 0,$$
$$B_3 = \frac{1}{e}, \quad d = e + 1 \text{ and } b = 1.$$

One gets

$$F(x, y, z) = x^2 + y^2 + (z - 1/e)^2 \tag{23}$$

and

$$\frac{\dot{F}}{2} = \left(\frac{1}{e} - a\right)x^2 - y^2 - \left(\sqrt{c}z - \frac{1 + c/e}{2\sqrt{c}}\right)^2 + \frac{(1 - c/e)^2}{4c} \tag{24}$$

The maximum value of F satisfies the equation $\dot{F} = 0$.

$$\left(a - \frac{1}{e}\right)x^2 + y^2 + \left(\sqrt{c}z - \frac{(1 + c/e)}{2\sqrt{c}}\right)^2 = \frac{(1-c/e)^2}{4c} \tag{25}$$

Let $t = \frac{1}{e}$, using the Lagrange multiplier method, we can get the maximum value under the condition of $\dot{F} = 0$, then define the Lagrange function.

$$G = x^2 + y^2 + (z - t)^2 + \lambda\left(-(a - t)x^2 - y^2 - \left(\sqrt{c}z - \frac{1 + tc}{2\sqrt{c}}\right)^2 + \frac{(1 - tc)^2}{4c}\right) \tag{26}$$

The partial derivative of the equation (26) can be obtained as.

$$\frac{\partial G}{2\partial x} = (1 - \lambda a + \lambda t)x = 0 \tag{27}$$

$$\frac{\partial G}{2\partial y} = (1 - \lambda)y = 0 \tag{28}$$

$$\frac{\partial G}{2\partial z} = z(1-\lambda c) + \frac{\lambda(1+bc)}{2} - b = 0 \tag{29}$$

$$\frac{\partial G}{2\partial \lambda} = (t-a)x^2 - y^2 + \left(\frac{1+tc}{2\sqrt{c}} - \sqrt{c}z\right)^2 + \frac{(1-tc)^2}{4c} = 0 \tag{30}$$

and then the extremum of the equation (23) is disscussed based on whether $\lambda c - 1$ is zero.

Case 2.1: When $\lambda c - 1 \neq 0, a \neq t$.

Case 2.1.1: When $\lambda = 1, \lambda \neq \frac{1}{a-t}$.

By solving (27) and (29), one obtains $x = 0$ and $z = \frac{1+tc-2t}{2(c-1)}$. Taking the result into the function (30), one obtains $y^2 = \frac{(c-2)(1-tc)^2}{4(c-1)^2}$. By calculation, we can get

$$F_{\max} = \frac{(1-tc)^2}{4(c-1)}.$$

Case 2.1.2: When $\lambda \neq 1, \lambda = \frac{1}{a-t}$.

By solving the equations (278), (29) and (30), one obtains

$$F_{\max} = \frac{(1-tc)^2}{4(c-a+t)^2(a-t)}.$$

Case 2.1.3: When $\lambda = 1, \lambda = \frac{1}{a-t}$.

By solving equation (29) and (30), one obtains

$$F_{\max} = \frac{(1-tc)^2}{4(c-1)}.$$

Case 2.1.4: When $\lambda \neq 1, \lambda \neq \frac{1}{a-t}$.

By solving the equations (27), (28), (29) and (30), one obtains

$$F_{\max} = \left(\frac{1-tc}{c}\right)^2.$$

Case 2.2: When $\lambda c - 1 = 0, a \neq t$.

Case 2.2.1: When $c \neq 1, c \neq a - t$.

By solving the equations (27), (28) and (29), we can get $(x, y, z) = (0, 0, t)$ or $(x, y, z) = (0, 0, t)$. However, $(x, y, z) = (0, 0, t)$ is not appropriate since $F(x, y, z) \neq 0$. When $(x, y, z) = \left(0, 0, \frac{1}{c}\right)$, one obtains

$$F_{\max} = \left(\frac{1-bc}{c}\right)^2.$$

Case 2.2.2: When $c = 1, c \neq a - t$. unsolvable.

Case 2.2.3: When $c \neq 1, c = a - t$. unsolvable.

Case 2.2.4: When $c = 1, c = a - t$. unsolvable.

So, when the parameters $a = -0.88, b = 1, c = 0.36, d = -0.5$ and $e = -1.5$,

$$F_{\max} = \left(\frac{1-tc}{c}\right)^2 = 3.44^2,$$

and the ultimate boundary of the system (5) is $x^2 + y^2 + (z + 2/3)^2 \leq 3.44^2$, as shown in Fig. 5.

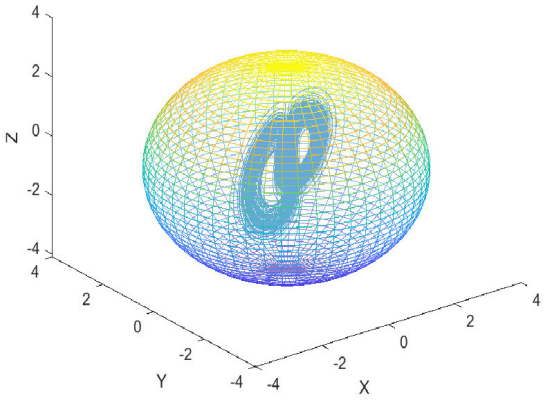

FIGURE 5. The ultimate boundary.

V. DIVERGENCE MEASURE

According to the stability of the equilibrium point and ultimate boundary obtained in the above sections, the divergence of system (5) is analyzed when the initial point is selected outside the ultimate boundary.

The divergence of the system (5) can be expressed as

$$\nabla \cdot V = \frac{\partial \dot{x}}{\partial x} + \frac{\partial \dot{y}}{\partial y} + \frac{\partial \dot{z}}{\partial z} = -a + z - 1 - c \tag{31}$$

which is related to the parameters a and c, and variable z. The average divergence is defined as follows.

$$\nabla \cdot \bar{V} = \frac{\partial \dot{x}}{\partial x} + \frac{\partial \dot{y}}{\partial y} + \frac{\partial \dot{z}}{\partial z} = \frac{1}{N}\sum_{t=1}^{N} \nabla z(t) - a - 1 - c \tag{32}$$

When $a = -0.88, b = 1, c = 0.36, d = -0.5$ and $e = -1.5$, the system average divergence can be obtained as

$$\nabla \cdot \bar{V} = \frac{\partial \dot{x}}{\partial x} + \frac{\partial \dot{y}}{\partial y} + \frac{\partial \dot{z}}{\partial z} == -0.48 + \frac{1}{N}\sum_{t=1}^{N} \nabla z(t) \tag{33}$$

and we can get $\bar{z} = -0.3236$, so the average divergence of the system is

$$\nabla \cdot \bar{V} = \frac{\partial \dot{x}}{\partial x} + \frac{\partial \dot{y}}{\partial y} + \frac{\partial \dot{z}}{\partial z} = -a + \bar{z} - 1 - c = -0.8036 < 0 \tag{34}$$

Hence, the system is dissipative, that is, a volume element with an initial volume $V(0)$ converges to volume element $V(0)e^{-(a-\bar{z}+1+c)t_0}$ at time t_0, which means that when $t \to \infty$, each volume element including system trajectory shrinks to 0 at an exponential rate $-(a - \bar{z} + 1 + c)$.

At the initial time, the divergence of the system will be affected by the initial point. When the initial point $z_0 > 0.48$, the initial divergence of the system is greater than 0, otherwise, it is less than 0, which means that the contraction and expansion state of each volume element including the trajectory of the system is uncertain at the initial time.

When the initial value is selected as $x_0 = (0.7459, 0.5583, z_0)$, the bifurcation diagram of the system can be obtained by changing the initial point, as shown in Fig. 6.

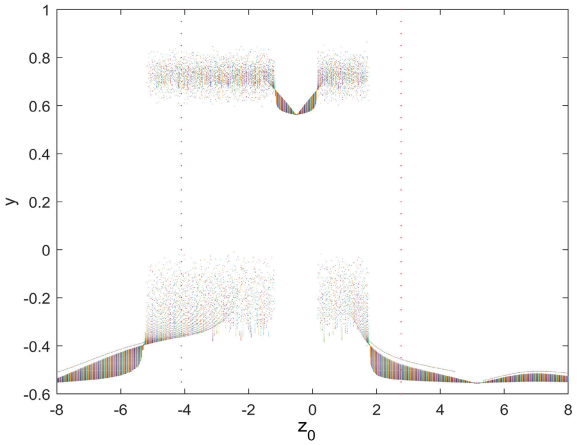

FIGURE 6. The bifurcation diagram of variable initial value.

The red dashed lines in Fig. 6 are the upper and lower bounds of the ultimate boundary, $z_1 = 2.7733$ and $z_2 = -4.1067$, respectively. In this paper, we only discuss the case that the initial point is selected outside the ultimate boundary of the system (5), because there are two states within the ultimate boundary of the system, that is, chaos and quasi period. And the quasi period is two quasi period states, converging to the equilibrium point E_3 and E_4 respectively, so it is hard to quantify the volume changes of the system.

In order to quantify the variation of divergence, when the initial point is selected outside the ultimate boundary, two indicators D and K are proposed to measure divergence.

Definition 1: Select the state x_m of the system at time mT, where T is the step size; the distance D between the state x_m of the system and the equilibrium point x_e in the $x - y$ plane, is used to indicate the distance between the current state of the system and the attractor, which ia also called the relative attractor distance. Here, x_e equilibrium point that the trajectory of the system converges to first. Hence D is defined as

$$D = \sqrt{(x_m - x_e)^2 + (y_m - y_e)^2} \tag{35}$$

We select the data of the first 0.1 s, the step size is 0.001 s, for indicating the distance between the current state of the system (5) and the attractor.

Definition 2: Select the states x_n and x_m of the system (5) at time nT and mT. The direction vector between x_n and x_m is used to represent the trend of volume contraction in phase space, which is called contraction trend variable K. The equation expression of K is

$$K = (|x_n - x_m|, |y_n - y_m|, |z_n - z_m|) \tag{36}$$

The selection of n and m depends on the actual situation. In order to show the trend of system contraction, the data from 0.001 s to 0.05 s and the step size 0.001 s are selected to show the change of system phase space volume at the initial time.

Three different initial points outside the ultimate boundary are selected as $x_{01} = (0.7459, 0.5583, -6)$, $x_{02} = (0.7459, 0.5583, -4.5)$ and $x_{03} = (0.7459, 0.5583, 4)$, and

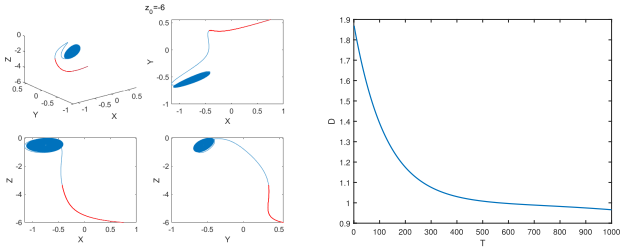

(a) The phase diagram (b) The diagram of D

FIGURE 7. The system phase diagram and diagram of D.

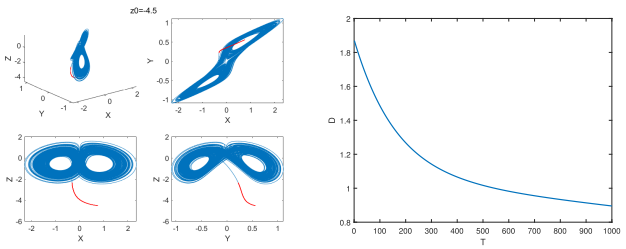

(a) The phase diagram (b) The diagram of D

FIGURE 8. The system phase diagram and diagram of D.

the system is quasi periodic, chaotic and quasi periodic, respectively. Then the change of phase space volume is analyzed when these three initial points are selected.

Case 1: When $x_{01} = (0.7459, 0.5583, -6)$, the divergence at the initial time of the system is

$$\nabla \cdot V_0 = \frac{\partial \dot{x}}{\partial x} + \frac{\partial \dot{y}}{\partial y} + \frac{\partial \dot{z}}{\partial z} = -a + z_0 - 1 - c = -6.48 < 0 \tag{37}$$

the phase diagram of the system and the diagram of D are shown in Fig. 7.

The red curve in Fig. 7(a) is the data of the first 1 s. We can clearly see the shrinking of the volume element from Fig. 7(a). And D gradually decreases, as time goes by, as can be seen from Fig. 7(b).

Case 2: When $x_{02} = (0.7459, 0.5583, -4.5)$, the divergence at the initial time of the system (5) is

$$\nabla \cdot V_0 = \frac{\partial \dot{x}}{\partial x} + \frac{\partial \dot{y}}{\partial y} + \frac{\partial \dot{z}}{\partial z} = -a + z_0 - 1 - c = -4.98 < 0 \tag{38}$$

The phase diagram of the system and the diagram of D are shown in Fig. 8.

In Fig. 8(a), the red curve is the data of the first 1 s. As can be seen from Fig. 8(a), the volume element gradually shrinks as time goes by. It can be seen from Fig. 8(b) that D gradually decreases.

Case 3: When $x_{03} = (0.7459, 0.5583, 4)$, the divergence at the initial time of the system is

$$\nabla \cdot V_0 = \frac{\partial \dot{x}}{\partial x} + \frac{\partial \dot{y}}{\partial y} + \frac{\partial \dot{z}}{\partial z} = -a + z_0 - 1 - c = 3.52 > 0 \tag{39}$$

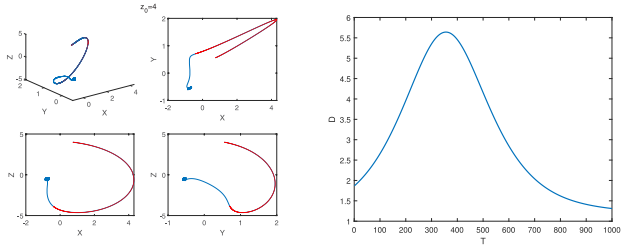

(a) The phase diagram (b) The diagram of D

FIGURE 9. The system phase diagram and diagram of D.

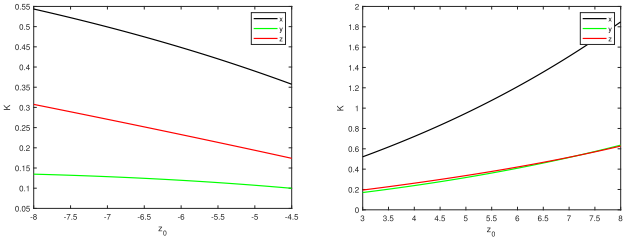

(a) $-8 \le z_0 \le -4.5$ (b) $3 \le z_0 \le 8$

FIGURE 10. The sequence diagram of K.

The phase diagram of the system (5) and the diagram of D are shown in Fig. 9.

The red curve in Fig. 9(a) is the data of the first 1 s. It can be seen that the volume element is expanded outwards at the beginning, and then the volume product element starts to contract under the effect of attractor in Fig. 9(a). From Fig. 9(b), we can also find that D increases firstly, and then decreases gradually.

The sequence diagram of K at $3 \le z_0 \le 8$ and $-8 \le z_0 \le -4.5$ are shown in Fig. 10, which shows the effect of $|z_0|$ on the contraction rate.

From Fig. 10(a), it can be seen that when $-8 \le z_0 \le -4.5$, that is, $4.5 \le |z_0| \le 8$, the value of K changes monotonously with the decrease of $|z_0|$, that is, the initial divergence of the system (5) decreases with the decrease of $|z_0|$, and the rate of contraction decreases. Similarly, when $3 \le z_0 \le 8$, that is, $3 \le |z_0| \le 8$, the value of K also changes monotonously with the decrease of $|z_0|$, that is, the initial divergence of the system increases with the increase of $|z_0|$, and the expansion rate increases.

From the above three cases, the influence of initial points outside the ultimate boundary on each volume element is revealed. When the initial divergence of the system is positive, the trajectory of the system (5) will expand firstly, but the average divergence of the system (5) is still negative, so the system trajectory will eventually be attracted to the chaotic attractor. Meanwhile, when the initial divergence of the system is negative, the trajectory of the system will firstly contract and then finally be attracted to the chaotic attractor. The three-dimensional diagram of D is drawn in Fig. 11, to further analyze the influence of different initial points on the volume change in the phase space.

The green area is the part where the indicator D is greater than 0, and the red area is the part where the indicator D is

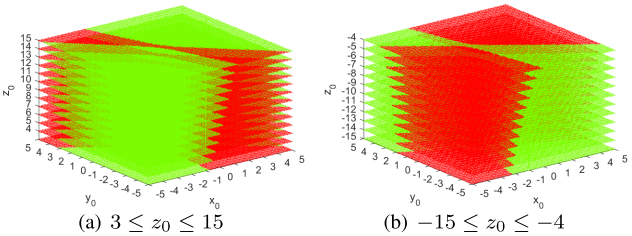

(a) $3 \le z_0 \le 15$ (b) $-15 \le z_0 \le -4$

FIGURE 11. The three-dimensional diagram of D.

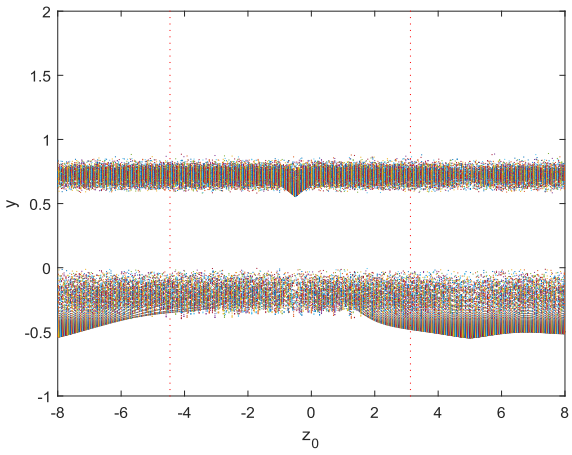

FIGURE 12. The bifurcation diagram on variable initial value.

less than 0 in Fig. 11. In Fig. 11 (a), $3 < Z_0 < 15$, the initial values in the green area achieve the phase space volume that expands first and then contracts. In Fig. 11 (b), $-15 < Z_0 < -4$, the initial values in the red area can achieve the extracted phase space volume.

It is necessary to analyze the change of system volume element. Without loss of generality, $c = 0.32$ is chosen to analyze the influence of the equilibrium point stability on the divergence. When $c = 0.32$, the system is chaotic, but the three equilibrium points are all unstable equilibrium points, and the system divergence is still related to the value of the variable z. Here, the initial point is selected outside the ultimate boundary of the system (5). Firstly, the bifurcation diagram of the system (5) is drawn in Fig. 12, when the initial point is $x_0 = (0.7396, 0.5534, z0)$.

The red lines $z_1 = 3.1253$ and $z_2 = -4.4587$, in Fig. 12, are the upper and lower boundary of the ultimate boundary. We can find the system is always chaotic from Fig. 12. Here, $x_{01} = (0.7396, 0.5534, 4)$ and $x_{02} = (0.7396, 0.5534, -6)$ are chosen as two cases to study whether the stability of the equilibrium point has impact on the volume change of the system.

Case 1: When $x_{01} = (0.7396, 0.5534, 4)$, the initial divergence of the system (5) is

$$\nabla \cdot V_0 = \frac{\partial \dot{x}}{\partial x} + \frac{\partial \dot{y}}{\partial y} + \frac{\partial \dot{z}}{\partial z} = -a + z_0 - 1 - c = 3.56 > 0 \tag{40}$$

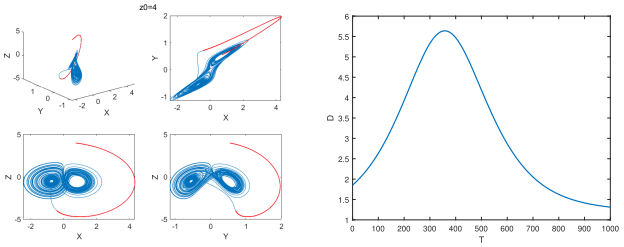

(a) The phase diagram (b) The diagram of D

FIGURE 13. The system phase diagram and diagram of D.

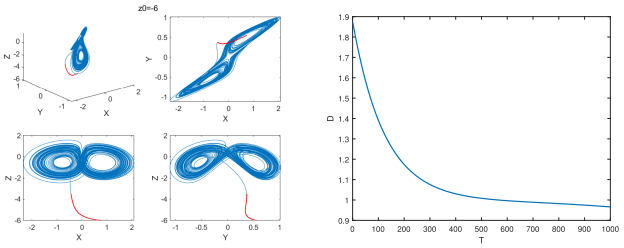

(a) The phase diagram (b) The diagram of D

FIGURE 14. The system phase diagram and diagram of D.

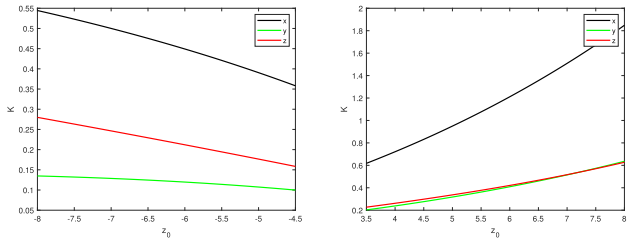

(a) $-8 \leq z_0 \leq -4.5$ (b) $3.5 \leq z_0 \leq 8$

FIGURE 15. The sequence diagram of K.

The phase diagram of the system and the diagram of D are shown in Fig. 13.

Case 2: When $x_{02} = (0.7396, 0.5534, -6)$, the initial divergence of the system (5) is

$$\nabla \cdot V_0 = \frac{\partial \dot{x}}{\partial x} + \frac{\partial \dot{y}}{\partial y} + \frac{\partial \dot{z}}{\partial z} = -a + z_0 - 1 - c = -6.44 < 0 \tag{41}$$

The phase diagram of the system (5) and the diagram of D are shown in Fig. 14.

It can be seen from Figs. 13 and 14 that the value of variable D changes as time goes by, obviously, it meets the previous conclusion.

The sequence diagram of K of the system (5) at $-8 \leq z_0 \leq -4.5$ and $3.5 \leq z_0 \leq 8$ are shown in Fig. 15. It can be seen from Fig. 15 that the volume of the phase space of the system contracts when the initial divergence is less than 0, while the volume expands first and then contracts when the initial divergence is greater than 0, obviously which meets the previous conclusion at $c = 0.36$.

When $c = 0.32$, the three-dimensional diagram of D is given in Fig. 16.

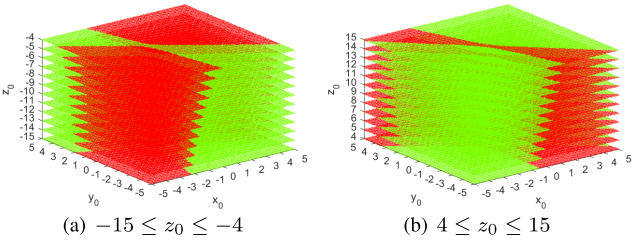

(a) $-15 \leq z_0 \leq -4$ (b) $4 \leq z_0 \leq 15$

FIGURE 16. The three-dimensional diagram of D.

As can be seen from Fig. 16, when $c = 0.36$ and $c = 0.32$ the three-dimensional diagrams of D are similar. From the analyses of $c = 0.36$ and $c = 0.32$, it can be found that when the divergence of the system (5) is related to the variable z, the volume contraction and expansion is related to the selection of the initial point, which is outside the ultimate boundary of the system. When the initial divergence is greater than 0, the volume of the system (5) expands first and then contracts. When the initial divergence is less than 0, the volume of the system (5) shrinks as time goes by. Moreover, the contraction rate of phase space volume is related to the initial point of the system (5).

VI. CONCLUSION

In this paper, a three-dimensional dissipative system was proposed and the mechanism of the system is analyzed by contrasting it with the Kolmogorov form. Furthermore, it was found that the system divergence is related to the variable z. In order to analyze the influence of divergence on the system dynamics, and the ultimate bound and the stability of the equilibrium points are studied. Although the divergence of the system is related to the variable z, the average divergence of the system is still negative and the system is dissipative. Then two new indicators D and K were introduced to analyze the influence of divergence on the system dynamics, when the initial point is outside the ultimate boundary. And it was found that when the initial divergence is less than 0, the system volume is keeping on contracting; when the initial divergence is greater than 0, the system volume expands first and then contracts. The divergence measurement method proposed in this paper for the initial state of system can effectively analyze the influence of divergence on the proposed system, which is worth studying for this kind of special system, especially for the two wing attractor.

REFERENCES

[1] P. L. Christiansen, M. P. Sørensen, and A. C. Scott, "Nonlinear science at the dawn of the 21st century," *Lect. Notes Phys.*, vol. 542, no. 3, pp. 395–407, 2000.

[2] E. N. Lorenz, "Deterministic nonperiodic flow," *J. Atmos. Sci.*, vol. 20, no. 2, pp. 130–141, Mar. 1963.

[3] M. Varadharajan, P. Duraisamy, and A. Karthikeyan, "Route to chaos and bistability analysis of quasi-periodically excited three-leg supporter with shape memory alloy," *Complexity*, vol. 2020, pp. 1–10, Sep. 2020.

[4] Q. Wu and G. Qi, "Homoclinic bifurcations and chaotic dynamics of non-planar waves in axially moving beam subjected to thermal load," *Appl. Math. Model.*, vol. 83, pp. 674–682, Jul. 2020.

[5] J. Alidousti, "Stability and bifurcation analysis for a fractional prey–predator scavenger model," *Appl. Math. Model.*, vol. 81, pp. 342–355, May 2020.

[6] G. Qi, J. Hu, and Z. Wang, "Modeling of a Hamiltonian conservative chaotic system and its mechanism routes from periodic to quasiperiodic, chaos and strong chaos," *Appl. Math. Model.*, vol. 78, pp. 350–365, Feb. 2020.
[7] J. Kengne, Z. T. Njitacke, and H. B. Fotsin, "Dynamical analysis of a simple autonomous jerk system with multiple attractors," *Nonlinear Dyn.*, vol. 83, nos. 1–2, pp. 751–765, Jan. 2016.
[8] H. Li, H. Bao, L. Zhu, B. Bao, and M. Chen, "Extreme multistability in simple area-preserving map," *IEEE Access*, vol. 8, pp. 175972–175980, 2020.
[9] Q. Lai, "A unified chaotic system with various coexisting attractors," *Int. J. Bifurcation Chaos*, vol. 31, no. 1, Jan. 2021, Art. no. 2150013.
[10] B. C. Bao, Q. Xu, H. Bao, and M. Chen, "Extreme multistability in a memristive circuit," *Electron. Lett.*, vol. 52, no. 12, pp. 1008–1009, 2016.
[11] Q. Lai, Z. Wan, and P. D. K. Kuate, "Modelling and circuit realisation of a new no-equilibrium chaotic system with hidden attractor and coexisting attractors," *Electron. Lett.*, vol. 56, no. 20, pp. 1044–1046, Sep. 2020.
[12] C. R. Hens, R. Banerjee, U. Feudel, and S. K. Dana, "How to obtain extreme multistability in coupled dynamical systems," *Phys. Rev. E, Stat. Phys. Plasmas Fluids Relat. Interdiscip. Top.*, vol. 85, no. 3, p. 4, Mar. 2012.
[13] Q. Lai, Z. Wan, P. D. K. Kuate, and H. Fotsin, "Coexisting attractors, circuit implementation and synchronization control of a new chaotic system evolved from the simplest memristor chaotic circuit," *Commun. Nonlinear Sci. Numer. Simul.*, vol. 89, Oct. 2020, Art. no. 105341.
[14] Q. Lai, B. Norouzi, and F. Liu, "Dynamic analysis, circuit realization, control design and image encryption application of an extended Lü system with coexisting attractors," *Chaos, Solitons Fractals*, vol. 114, pp. 230–245, Sep. 2018.
[15] Y. Peng, K. Sun, and S. He, "Synchronization for the integer-order and fractional-order chaotic maps based on parameter estimation with JAYA-IPSO algorithm," *Eur. Phys. J. Plus*, vol. 135, no. 3, p. 12, Mar. 2020.
[16] M. G. Rosenblum, A. S. Pikovsky, and J. Kurths, "From phase to lag synchronization in coupled chaotic oscillators," *Phys. Rev. Lett.*, vol. 78, no. 22, pp. 4193–4196, Jun. 1997.
[17] V. N. Giap, Q. D. Nguyen, and S. C. Huang, "Synthetic adaptive fuzzy disturbance observer and sliding-mode control for chaos-based secure communication systems," *IEEE Access*, vol. 9, pp. 23907–23928, 2021.
[18] Y. Huang, X. Yuan, H. Long, X. Fan, and T. Cai, "Multistability of fractional-order recurrent neural networks with discontinuous and non-monotonic activation functions," *IEEE Access*, vol. 7, pp. 116430–116437, 2019.
[19] H. Li, Z. Hua, H. Bao, L. Zhu, M. Chen, and B. Bao, "Two-dimensional memristive hyperchaotic maps and application in secure communication," *IEEE Trans. Ind. Electron.*, early access, Sep. 15, 2021, doi: 10.1109/TIE.2020.3022539.
[20] H. Bao, Z. Hua, N. Wang, L. Zhu, M. Chen, and B. Bao, "Initials-boosted coexisting chaos in a 2-D sine map and its hardware implementation," *IEEE Trans. Ind. Informat.*, vol. 17, no. 2, pp. 1132–1140, Feb. 2021.
[21] F. Yang, J. Mou, K. Sun, and R. Chu, "Lossless image compression-encryption algorithm based on BP neural network and chaotic system," *Multimedia Tools Appl.*, vol. 79, nos. 27–28, pp. 19963–19992, Jul. 2020.
[22] B. Bao, P. Jiang, H. Wu, and F. Hu, "Complex transient dynamics in periodically forced memristive Chua's circuit," *Nonlinear Dyn.*, vol. 79, no. 4, pp. 2333–2343, Mar. 2015.
[23] C. Li, D. Lin, B. Feng, J. Lu, and F. Hao, "Cryptanalysis of a chaotic image encryption algorithm based on information entropy," *IEEE Access*, vol. 6, pp. 75834–75842, 2018.
[24] E. Dong, Z. Liang, S. Du, and Z. Chen, "Topological horseshoe analysis on a four-wing chaotic attractor and its FPGA implement," *Nonlinear Dyn.*, vol. 83, nos. 1–2, pp. 623–630, Jan. 2016.
[25] M. Elnawawy, F. Aloul, A. Sagahyroon, A. S. Elwakil, W. S. Sayed, L. A. Said, S. M. Mohamed, and A. G. Radwan, "FPGA realizations of chaotic epidemic and disease models including COVID-19," *IEEE Access*, vol. 9, pp. 21085–21093, 2021.
[26] X. Dai, T. Huang, Y. Huang, Y. Luo, G. Wang, and M. Xiao, "Chaotic behavior of discrete-time linear inclusion dynamical systems," *J. Franklin Inst.*, vol. 354, no. 10, pp. 4126–4155, Jul. 2017.
[27] W. Pan, X. Li, L. Wang, and Z. Yang, "Nonlinear response analysis of gear-shaft-bearing system considering tooth contact temperature and random excitations," *Appl. Math. Model.*, vol. 68, pp. 113–136, Apr. 2019.
[28] M. Qiao, F. Xu, and S. C. Saha, "Numerical study of the transition to chaos of a buoyant plume from a two-dimensional open cavity heated from below," *Appl. Math. Model.*, vol. 61, pp. 577–592, Sep. 2018.
[29] E. Dong, M. Yuan, C. Zhang, J. Tong, Z. Chen, and S. Du, "Topological horseshoe analysis, ultimate boundary estimations of a new 4D hyper-chaotic system and its FPGA implementation," *Int. J. Bifurcation Chaos*, vol. 28, no. 7, Jun. 2018, Art. no. 1850081.
[30] E. Dong, Z. Zhang, M. Yuan, Y. Ji, X. Zhou, and Z. Wang, "Ultimate boundary estimation and topological horseshoe analysis on a parallel 4D hyperchaotic system with any number of attractors and its multi-scroll," *Nonlinear Dyn.*, vol. 95, no. 4, pp. 3219–3236, Mar. 2019.
[31] G. Qi and J. Zhang, "Energy cycle and bound of Qi chaotic system," *Chaos, Solitons Fractals*, vol. 99, pp. 7–15, Jun. 2017.
[32] G. Leonov, A. Bunin, and N. Koksch, "Attractor localization of the Lorenz system," *Zeitschrift Angewandte Mathematik Mechanik*, vol. 67, no. 12, pp. 649–656, 1987.
[33] X. Liao, F. U. Yuli, and S. Xie, "On the new results of global attractive set and positive invariant set of the Lorenz chaotic system and the applications to chaos control and synchronization," *Sci. China*, vol. 48, no. 3, pp. 304–321, 2005.
[34] P. Swinnerton-Dyer, "Bounds for trajectories of the Lorenz equations: An illustration of how to choose Liapunov functions," *Phys. Lett. A*, vol. 281, nos. 2–3, pp. 161–167, Mar. 2001.
[35] D. Li, J.-A. Lu, X. Wu, and G. Chen, "Estimating the bounds for the Lorenz family of chaotic systems," *Chaos, Solitons Fractals*, vol. 23, no. 2, pp. 529–534, Jan. 2005.
[36] D. Li, J.-A. Lu, X. Wu, and G. Chen, "Estimating the ultimate bound and positively invariant set for the Lorenz system and a unified chaotic system," *J. Math. Anal. Appl.*, vol. 323, no. 2, pp. 844–853, Nov. 2006.
[37] P. Yu and X. Liao, "New estimations for globally attractive and positive invariant set of the family of the Lorenz systems," *Int. J. Bifurcation Chaos*, vol. 16, no. 11, pp. 3383–3390, Nov. 2006.
[38] P. Yu and X. X. Liao, "On the study of globally exponentially attractive set of a general chaotic system," *Commun. Nonlinear Sci. Numer. Simul.*, vol. 13, no. 8, pp. 1495–1507, Oct. 2008.
[39] Y. Shu and Y. Zhang, "Estimating the ultimate bound and positively invariant set for a generalized Lorenz system," *J. Chongqing Univ.*, vol. 7, no. 2, pp. 71–74, 2008.
[40] Y.-J. Sun, "Solution bounds of generalized Lorenz chaotic systems," *Chaos, Solitons Fractals*, vol. 40, no. 2, pp. 691–696, Apr. 2009.
[41] W.-X. Qin and G. Chen, "On the boundedness of solutions of the Chen system," *J. Math. Anal. Appl.*, vol. 329, no. 1, pp. 445–451, May 2007.
[42] X. Liao, Y. Pei, S. Xie, and Y. Fu, "Study on the global property of the Chua's system," *Int. J. Bifurcat. Chaos*, vol. 16, no. 10, pp. 2815–2841, 2006.
[43] D. Li, X. Wu, and J.-A. Lu, "Estimating the ultimate bound and positively invariant set for the hyperchaotic Lorenz–Haken system," *Chaos, Solitons Fractals*, vol. 39, no. 3, pp. 1290–1296, Feb. 2009.
[44] S. Cang, A. Wu, R. Zhang, Z. Wang, and Z. Chen, "Conservative chaos in a class of nonconservative systems: Theoretical analysis and numerical demonstrations," *Int. J. Bifurcation Chaos*, vol. 28, no. 7, Jun. 2018, Art. no. 1850087.
[45] I. L. Aleiner and A. I. Larkin, "Divergence of classical trajectories and quantum chaos," *Chaos, Solitons Fractals*, vol. 8, nos. 7–8, pp. 1179–1204, Jul. 1997.
[46] A. Kowalewska-Kudłaszyk, J. K. Kalaga, W. Leoński, and V. C. Long, "Kullback–Leibler quantum divergence as an indicator of quantum chaos," *Phys. Lett. A*, vol. 376, no. 15, pp. 1280–1286, Mar. 2012.
[47] G. K. Nave, P. J. Nolan, and S. D. Ross, "Trajectory-free approximation of phase space structures using the trajectory divergence rate," *Nonlinear Dyn.*, vol. 96, no. 1, pp. 685–702, Apr. 2019.
[48] J. C. Sprott, "Some simple chaotic flows," *Phys. Rev. E, Stat. Phys. Plasmas Fluids Relat. Interdiscip. Top.*, vol. 50, no. 2, pp. R647–R650, Aug. 1994.
[49] G. Qi and X. Liang, "Mechanism and energy cycling of the Qi four-wing chaotic system," *Int. J. Bifurcation Chaos*, vol. 27, no. 12, Nov. 2017, Art. no. 1750180.
[50] V. I. Arnold, "Kolmogorov's hydrodynamic attractors," *Proc. Roy. Soc. London, A, Math. Phys. Sci.*, vol. 434, no. 1890, pp. 19–22, 1991.
[51] H. Jia, W. Shi, and G. Qi, "Coexisting attractors, energy analysis and boundary of Lü system," *Int. J. Bifurcation Chaos.*, vol. 30, no. 3, pp. 2771–2776, 2020.
[52] H. Jia, W. Shi, L. Wang, and G. Qi, "Energy analysis of sprott—A system and generation of a new Hamiltonian conservative chaotic system with coexisting hidden attractors," *Chaos, Solitons Fractals*, vol. 133, Apr. 2020, Art. no. 109635.

[53] W. Xue, Y. Li, S. Cang, H. Jia, and Z. Wang, "Chaotic behavior and circuit implementation of a fractional-order permanent magnet synchronous motor model," *J. Franklin Inst.*, vol. 352, no. 7, pp. 2887–2898, Jul. 2015.
[54] W. Xue, M. Zhang, S. Liu, Y. Li, and S. Cang, "Mechanical analysis and ultimate boundary estimation of the chaotic permanent magnet synchronous motor," *J. Franklin Inst.*, vol. 356, no. 10, pp. 5378–5394, Jul. 2019.
[55] C. Li, H. Li, and Y. Tong, "Analysis of a novel three-dimensional chaotic system," *Optik*, vol. 124, no. 13, pp. 1516–1522, Jul. 2013.
[56] C. Li and J. C. Sprott, "An infinite 3-D quasiperiodic lattice of chaotic attractors," *Phys. Lett. A*, vol. 382, no. 8, pp. 581–587, Feb. 2018.

ENZENG DONG was born in Hebei, China, in 1977. He received the Ph.D. degree in operational research and cybernetics from Nankai University, Tianjin, China, in 2006. He is currently a Professor with the School of Electrical and Electronic Engineering, Tianjin University of Technology. His research interests include intelligent control theory and applications and brain–computer interface (BCI).

HUI YU was born in Fuyang, Anhui, China, in 1996. He received the B.S. degree in automation from the Tianjin University of Technology, in 2019, where he is currently pursuing the M.S. degree. His research interests include nonlinear dynamics and chaos theory.

JIGANG TONG was born in Jinzhou, Liaoning, China, in 1975. He received the Ph.D. degree in control theory and control engineering from Nankai University, Tianjin, China, in 2010. He is currently a Lecturer with the School of Electrical and Electronic Engineering, Tianjin University of Technology. His research interests include gait analysis, intelligent control, and embedded systems.

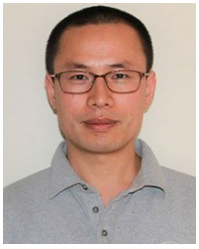

ZENGHUI WANG (Member, IEEE) received the Ph.D. degree in control theory and control engineering from Nankai University, China, in 2007. He is currently a Professor with the Department of Electrical and Mining Engineering, University of South Africa (UNISA), South Africa. His research interests include the Internet of Things, nonlinear control, engineering optimization, artificial intelligence, chaos, and industry 4.0.